Automatic Change Detection in Multitemporal SAR Orthoimages

Rafael A. S. Rosa* **, David Fernandes, João Bosco Nogueira Jr.*****

* Bradar Indústria S/A
** Instituto Tecnológico de Aeronáutica
*** Santo Antônio Energia S/A

Abstract. Forest monitoring is a major concern today due to climate changes, conservation of fauna and flora and to the lack of water. Therefore, several environmental monitoring techniques have been developed and used to detect changes in the scenes. However, the main techniques have limitations related to weather conditions and does not have the expected effect. The use of SAR (Synthetic Aperture Radar) seems appropriate to detect changes due to its independence of atmospheric and lighting conditions. The SAR change detection is a process that uses SAR images acquired in the same geometric conditions but in different moment (multitemporal) to identify changes in the surface that occurred between two acquisitions. This paper presents a new method of change detection in multitemporal SAR orthoimages using the difference between them. The novelty of this method is the detection threshold definition: it is usually an orthoimages difference function, but in this method it is calculated using only one of the orthoimages. In addition, another novelty is the combined use of already known techniques: the speckle filtering, the normalization and the morph close operation. Experimental tests were conducted using real SAR data obtained by the airborne sensor OrbiSAR-2 from Bradar in the Amazon Forest and the results showed a higher accuracy than those found in the literature.

Keywords: Change detection, Multitemporal images, Synthetic aperture radar (SAR)

1. Introduction

One of the most important topics today is the climate change, and one of its main possible cause is the deforestation of rainforests around the world.

Just talking about the Amazon Forest, the last years deforestation average has been 5,000 km²/year (Bragança & Pegurier 2013). This scenario makes more and more organizations and institutions search surveillance methods for the reduction and prevention of deforestation. The most important Brazilian programs for this purpose are PRODES (Amazon Deforestation Monitoring Program) – the world's biggest forest monitoring program – and DETER (Real Time Deforestation Detection), both from INPE – National Institute for Space Research (O Eco 2013), doing the monitoring through satellite imagery. These programs have demonstrated their relevance, however they have two limitations due to their sensors: the resolution (15m) and the inability to map regions covered by clouds (Mileski 2008). At the beginning of these programs, there was a reduction of the Amazon deforestation rate, however after their limitations become known by the deforesters this rate has grown by using invisible techniques to that sensors: selective logging (isolated and scattered lumbering in order to hinder the identification); and the deforestation in rainy periods, when optical imaging sensors have restrictions due to clouds (Mileski 2008). That is why change detection by radar imaging, mainly SAR (Synthetic Aperture Radar), seems appropriate to equatorial and tropical forest monitoring due to its independence of weather conditions, without losing the high resolution. The purpose of this study was to develop an algorithm able to automatically detect changes in the surface in a time interval using SAR orthoimages from temporally spaced acquisitions, however with identical geometry (multitemporal). The goal was to create an efficient tool able to automatically identify regions where there was some kind of change, such as appearance of gaps in vegetation areas, trails, changes at forests borders, selective logging, growth of pastures, plantations and other dynamic land use. The following figures show examples of SAR orthoimages from the Bradar OrbiSAR-2 airborne sensor, obtained in the region of Porto Velho (Brazil) in 2013, provided by the Santo Antônio Energia S/A, with change indications through the RGB composition. *Figure 1* shows three images: (a) and (b) are SAR orthoimages obtained with 1-month interval between them; and (c) shows an RGB composition of these SAR orthoimages, wherein the R-band is composed of the older SAR orthoimage (a) and the G- and B-bands are equal and have the latest SAR orthoimage (b), in this way, the red regions are areas where there was less return of the radar signal in the second than in the first acquisition, in other words, they are areas where the targets were "disappeared" (cut trees), the cyan regions are areas where the opposite occurred, i.e., they are areas in which the return of the radar signal increased due to the "appearance" of targets (growth of pasture) and the gray regions are areas where there has been no significant change.

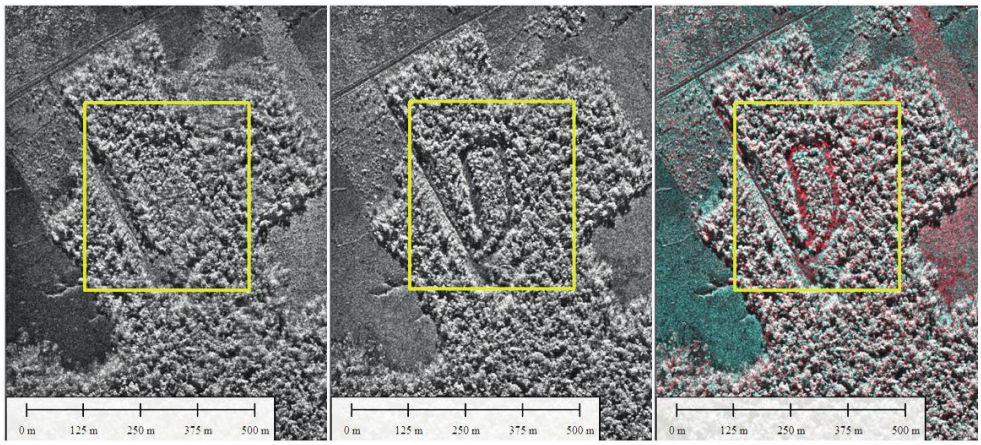

(a) (b) (c)

Figure 1. *SAR orthoimages obtained by OrbiSAR-2 sensor at 2012/09/23 (a) and 2012/10/20 (b); and the respective RGB composition (c).*

Figure 2 shows the SAR ability to detect the selective logging: this figure is also an RGB composition of two SAR orthoimages acquired with 1-month interval between them, generated with the same principle of the image (c) of *Figure 1*, this means that, the red regions represents the cut trees. In this image, the cyan regions are trees that were hidden in the first imaging and were exposed in the second. *Figure 3* (a) shows an RGB composition of two multitemporal acquisitions identifying a deforesting on the Madeira River banks and (b) is an aerial photography of this region obtained after the second of these acquisitions, confirming the detection.

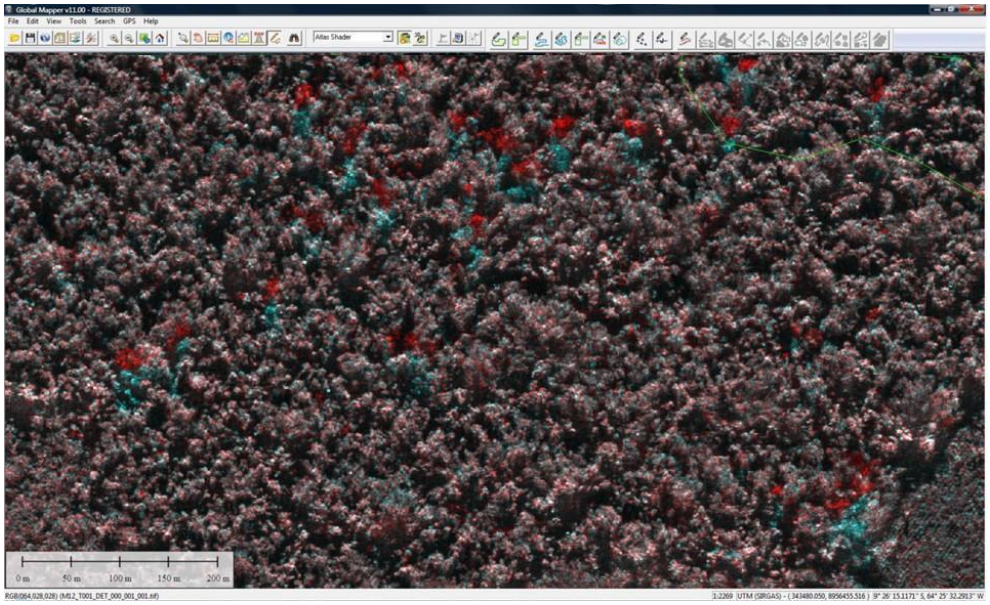

Figure 2. *RGB composition of multitemporal SAR orthoimages showing the selective logging in red and the appearance of targets in cyan.*

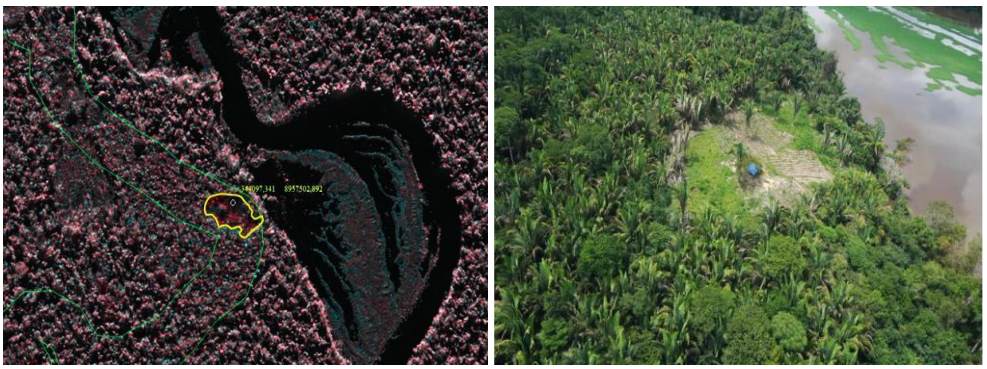

(a) (b)

Figure 3. *RGB composition of multitemporal SAR orthoimages showing a deforestation in the region delimited by the yellow contour (a) and corresponding aerial photograph of this deforested area (b).*

The objective of this work was to create an algorithm that, from multitemporal SAR orthoimages, is able to identify changes between them

and to produce binary masks that can be used for creating cartographic vectors, in an automatic and non- supervised way.

2. Review of Change Detection Methods

A simple method for change detection is the direct use of the difference or the ratio between the amplitude images, without the speckle filtering (Rignot et al. 1993, Grover et al. 1999, Dierking et al. 2002). Another proposed method was the use of the maximum likelihood (Lombardo et al. 2001). The speckle reduction through adaptive filters, the proper selection of a detection threshold and the logarithm of the ratio between two amplitude images were also treated by several studies (Bazi et al. 2005, Goodenough et al. 2006). Moser et al. (2007) used the Fischer Transform and the Markov Random Fields. Ranney & Khatri (2008) introduced the use of variable thresholds. Thayalan et al. (2009) used the entropy for change detection; the results were robust for radiometric errors. Pantze et al. (2010) used the difference between normalized amplitude images. Some studies used the segmentation and the classification for change detection from the classes changes (Servello et al. 2010, Wan & Jiao 2011), however, these methods are supervised. Thiele et al. (2012) did the segmentation using the forest borders through its shadows generated by the SAR geometry. Other works introduced the use of the Wavelet Domain (Wavelet Transform) and the Wavelet Fusion to generate the difference image, furthermore, they used the Gamma and the Rayleigh Distribution (Gong et al. 2012, Cui & Dactu 2012, Ma et al. 2012), and Gong et al. (2012) got the best existing result so far with an accuracy of 92.50% in some regions. Zheng & You (2013) proposed the use of neighborhoods rather than working with the pixel and also brought back the use of Gaussian Distribution. Zhang et al. (2013) used the difference image with Fuzzy Logic and Bayesian Inference. Wan et al. (2013) implemented the local connectivity. Bovolo et al. (2013) continued using the Wavelet Transform, but with the logarithm of the ratio of the amplitude images and variable thresholds, however, it should be need some kind of prior knowledge. Aiazzi et al. (2013) used more than two acquisitions simultaneously. And finally, Wang et al. (2013) got the best result recorded (accuracy of 96.91%) by using Hidden Markov Model (Triplet Markov Field) and Bayesian Inference (Bayesian Maximum Posterior Marginal Criterion). With this research, it was observed that the results vary greatly depending on the test area and in many cases the same method resulted in completely different measurements when applied to different regions.

3. Proposed Methodology

Let there be a set of multitemporal SAR orthoimages observed under the same geometric conditions (look angle, altitude, etc.):

$$X_T = \{x_t : t = 0,1,\ldots,T-1\}$$

where x_t is the t-th SAR orthoimage of size MxN, i.e., the SAR orthoimage acquired at the instant t. A pixel of this image x_t is represented by $x_t(m,n)$. The purpose is to detect changes between the consecutive orthoimages x_t and x_{t+1}. One notes that if changes were detected in consecutive moments, it is possible to detect them between any x_t and $x_{t+\Delta t}$, where $t+\Delta t < T$. This paper proposes a semiempirical method for change detection by the difference between SAR orthoimages.

The SAR orthoimages have a multiplicative noise called speckle. This noise interferes in the image texture and can harm processes of segmentation, classification, border detection and also change detection between images (Bazi et al. 2005). The first step of this method is precisely the reduction of this noise: one uses adaptive filters and, among these, we chose the Lee Filter (Lee 1980), for its ease of implementation and for having, on average, a good performance considering varied scenes (Sena et al. 2013). The filtered image is represented by:

$$y_t = [x_t]_{Lee}$$

Although the images were radiometrically corrected (Rosa 2011), they may contain “non-desirable” differences, in other words, differences that one does not want to detect as change. These "non-desirable" differences may be due to using different radars, different weather conditions, etc.; for example, if in one of the acquisitions the vegetation was wet due to rain, the radiometric response is different from one in which the vegetation is dry. Thus, the second stage of the proposed method performs a normalization of the images: the image y_{t+1} is normalized in relation to the image y_t, so they have the same average and the same standard deviation. The normalization procedure is shown below (Ilsever & Ünsalan 2012):

$$\tilde{y}_{t+1} = \frac{\sigma_t\left(y_{t+1} - \overline{y}_{t+1}\right)}{\sigma_{t+1}} + \overline{y}_t$$

where $\tilde{y}_{t+1}$ is the normalization of the image y_{t+1} in relation to the image y_t; $\overline{y_t}$ is the average of the image y_t; and σ_t is the standard deviation of the image y_t.

The third step of this method – (Rignot et al. 1993, Grover et al. 1999, Derking et al. 2002, Pantze et al. 2010, Zhang et al. 2013) – is to calculate the difference between the normalized images y_t e $\tilde{y}_{t+1}$:

$$d_t = \tilde{y}_{t+1} - y_t$$

Despite the Lee Filter and the normalization, some "non-desirable" differences between images may still exist, per example, speckle residue, amplitude variation due to fluctuations in reflectivity of a extensive target or due to several observation conditions of the same scene, etc., and in order that its detection does not influence the desired final result, in the fourth step, a threshold is applied to the difference image to create a binary mask. The usual procedure is to calculate a threshold depending on the difference image d_t, however, in this way there is still a high number of false change detections caused by the effects mentioned above. One solution to this problem is the calculation of a threshold proportional to the standard deviation of the normalized orthoimages (σ_t) instead of the standard deviation of the difference. A multiplicative factor a is also added to this threshold; it is the trade-detector regulator, in other words, it will adjust the detection and false alarms in the process of predicting changes in the scene. Thus, the threshold is defined by:

$$L_t = a.\sigma_t$$

Then one applies the calculated threshold L_t, creating a binary mask image:

$$w_t(m,n) = \begin{cases} 1; d_t(m,n) > L_{1,t} \\ 0; d_t(m,n) \leq L_{1,t} \end{cases}; m = 0,1,\ldots,M-1; n = 0,1,\ldots,N-1$$

Finally, in order to join regions that are close to each other in the mask image w_t, the fifth and final step is the dilation and the erosion of the “islands” inside this mask image:

$$\widehat{w}_t = \left[[w_t]_{Dilata\ ção}\right]_{Erosão}$$

Figure 4 illustrates the dilation and erosion process of binary mask image. It is possible to see the dilation increases the "islands" uniting them with their closest neighbors (b), and the erosion is otherwise, but unable to separate those are strongly united because they were initially very close to each other (c). This process set of dilation and erosion, in this sequence, is called morph close operation (INPE 2014). The binary mask image $\hat{w}_t$ is the final result of the proposed method, and it can be used as raw data for generating cartographic vectors.

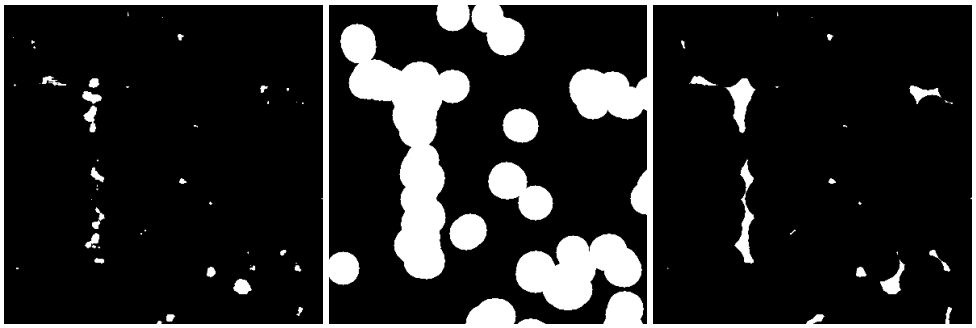

(a) (b) (c)

Figure 4. *Morph close operation: original image (a), image after dilation (b) and final image after erosion (c).*

4. Experimental Results

The proposed change detection algorithm was implemented in IDL (*Interactive Data Language*) and experiments have been performed using multitemporal SAR orthoimages provided by Santo Antônio Energia S/A acquired by the airborne sensor OrbiSAR-2 from Bradar. These multitemporal images were collected at the X-band monthly since September 2012 in the Amazon Forest (Porto Velho-RO) and processed in São José dos Campos-SP by Bradar, with the configuration shown in *Table 1*.

	OrbiSAR-2
Aircraft	Turbo-commander
Altitude	6086.62 m
Wavelenght	3.125 cm (X-band)
Off-nadir Angle	20º
Swath Width	14 km
Planimetric Resolution	1.0 m

Table 1. *OrbiSAR-2 sensor configuration.*

The used orthoimages cover an area of 2,938.59km² and they were acquired on March 18, 2013 (t) and May 16, 2013 ($t+1$) with 1.0m planimetric resolution. *Figure 5* shows a 1km² section of the original orthoimages x_t (a) and x_{t+1} (b).

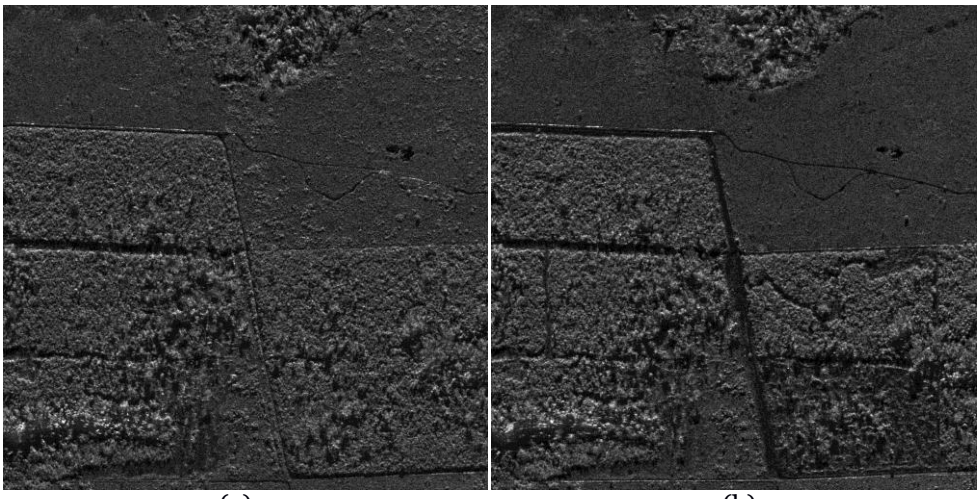

(a) (b)

Figure 5. *Original SAR orthoimages x_t (a) and x_{t+1} (b).*

The validation of the proposed method has been done by comparison with manually created reference data. This reference data was created by experienced operators from the analysis of multitemporal acquisitions and RGB compositions (*Figure 6*).

The parameters have been set up empirically: Lee filter with a square window of 5 pixels, detection threshold with a = 1,20 and morph close operation (dilation and erosion) with circular structure with radius of 5 pixels. The equivalent section from the binary mask final image $\hat{w}_t$ is shown in *Figure 7*.

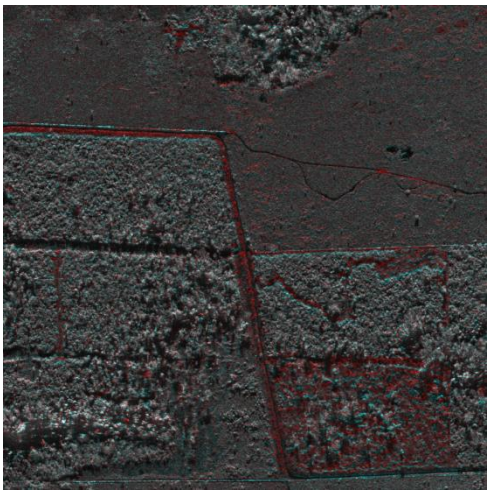

Figure 6. *RGB composition of the orthoimages x_t and x_{t+1}, with changes in red.*

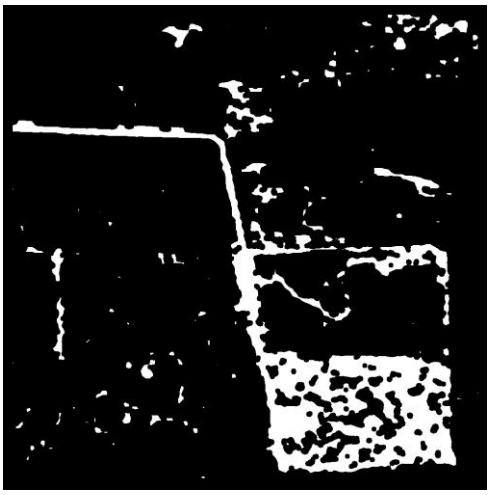

Figure 7. *Final image of the proposed method: binary mask.*

To measure the detection accuracy compared to the reference, one selected randomly 20 pairs of multitemporal SAR orthoimages with 0,25 km² (500 x 500 pixels) non-neighboring and non-intersecting each other from this area. The accuracy was calculated for all the selected regions and the average accuracy is 97.49% (*Table 2*).

Region	Accuracy (%)
1	99.17
2	99.55
3	99.05
4	96.05
5	98.79
6	98.09
7	95.42
8	99.59
9	99.53
10	98.54
11	87.42
12	99.14
13	97.36
14	99.15
15	90.27
16	99.30
17	99.44
18	97.38
19	99.35
20	97.23
Average	97.49
Standard Deviation	3.22

Table 2. *Experimental results.*

5. Conclusion

The multitemporal SAR image change detection methodology is a very relevant topic, but it is still an open problem in literature, or by the problem complexity, either by the wide variability of situations. The performed tests of this study showed a difficulty due to the specificity of each scene, including the landforms; this can be observed by the variation of results in *Table 2*. Ma et al. (2012) also observed this characteristic. Another factor which highlights the importance of this issue is the increased demand for change detection service and the consequent growth of the private sector investment in this area with several projects of multitemporal mapping and change detection in progress (Bradar 2014). Finally, in this work, a semiempirical methodology, that without being complex or computationally

onerous in terms of processing time, obtained great quality results as evidenced by the accuracy values presented in *Table 2*.

Acknowledgment

The authors would like to thank Santo Antônio Energia S/A for providing the multitemporal SAR orthoimages used in this work.

References

Aiazzi B, Alparone L, Baronti S, Garzelli A, Zoppetti C (2013) Nonparametric change detection in multitemporal SAR images based on mean-shift clustering. IEEE Transactions on Geoscience and Remote Sensing 51: 2022-2031

Bazi Y, Bruzzone L, Melgani F (2005) An unsupervised approach based on the generalized gaussian model to automatic change detection in multitemporal SAR images. IEEE Transactions on Geoscience and Remote Sensing, 43: 874-887

Bovolo F, Marin C, Bruzzone L (2013) A hierarchical approach to change detection in very high resolution SAR images for surveillance applications. IEEE Transactions on Geoscience and Remote Sensing 51: 2042-2054

Bradar Indústria S/A (2014) Sensoriamento remoto. http://www.bradar.com.br/sensoriamento-remoto.html. Accessed 3 April 2014

Bragança D, Pegurier E (2013) Especialistas comentam o aumento do desmatamento na Amazônia. http://www.oeco.org.br/noticias/27784-especialistas-comentam-o-aumento-do-desmatamento-na-amazonia. Accessed 3 April 2014

Cui S, Dactu M (2012) Statistical wavelet subband modeling for multi-temporal SAR change detection. IEEE Journal of Selected Topics in Applied Earth Observations and Remote Sensing 5: 1095-1109

Dierking W, Skriver H (2002) Change detection for thematic mapping by means of airborne multitemporal polarimetric SAR imagery. IEEE Transactions on Geoscience and Remote Sensing 40: 618-636

Gong M, Zhou Z, Ma J (2012) Change detection in synthetic aperture radar images based on image fusion and fuzzy clustering. IEEE Transactions on Image Processing 21: 2141-2151

Ilsever M, Ünsalan C (2012) Two-dimensional change detection methods – remote sensing applications. Springer London Heidelberg New York Dordrecht, New York

INPE (2014) Teoria: processamento de imagens. http://http://www.dpi.inpe.br/spring/teoria/filtrage/filtragem.htm. Accessed 17 March 2014

Lee JS (1980) Digital image enhancement and noise filtering by use of local statistics. IEEE Transactions on Pattern Analysis and Machine Intelligence 2

Lombardo P, Oliver CJ (2001) Maximum likelihood approach to the detection of changes between multitemporal SAR images. IEE Proceedings – Radar, Sonar Navigation 148: 200-210

Ma J, Gong M, Zhou Z (2012) Wavelet fusion on ratio images for change detection in SAR images. IEEE Geoscience and Remote Sensing Letters 9: 1122-1126

Mileski A (2008) DETER, PRODES e o desmatamento na Amazônia. http://panoramaespacial.blogspot.com.br/2008/08/deter-prodes-e-o-desmatamento-na.html. Accessed 3 April 2014

Moser G, Serpico S, Vernazza G (2007) Unsupervised change detection from multichannel SAR images. IEEE Geoscience and Remote Sensing Letters 4: 278-282

O Eco (2013) INPE comemora aniversário e celebra 25 anos do PRODES. http://www.oeco.org.br/noticias/27506-inpe-comemora-52-anos-de-existencia. Accessed 3 April 2014

Pantze A, Fransson JES (2010) Forest change detection from L-band satellite images using iterative histogram matching and thresholding together with data fusion. IGARSS 2010 Proceedings: 1226-1229, Honolulu

Ranney KI, Khatri HC (2008) Modified difference change detector for small targets in SAR imagery. IEEE Transactions on Aerospace and Electronic Systems 44: 57-76

Rignot EJM, Zyl JJ (1993) Change detection techniques for ERS-1 SAR data. IEEE Transactions on Geoscience and Remote Sensing 31: 896-906

Rosa RAS (2009) Correção radiométrica de imagens de radar de abertura sintética aerotransportado. Tese de Mestrado, Divisão de Engenharia Eletrônica, Instituto Tecnológico de Aeronáutica, São José dos Campos

Sena EF, Pereira TSM, Rosa ANCS (2013) Análise de filtragem do ruído speckle em imagens do radar de abertura sintética do SIPAM. Anais do XVI Simpósio Brasileiro de Sensoriamento Remoto: 8390-8396, Foz do Iguaçu

Servello EL, Kuplich TM, Shimabukuro YE (2010) Tropical land cover change detection with polarimetric SAR data. IGARSS 2010 Proceedings: 1477-1480, Honolulu

Thayalan A, Abas FS, Koo VC (2009) Automatic change detection of Belum-Temengor forested area using multitemporal SAR images. IEEE International Conference on Signal and Image Processing Applications: 318-321

Thiele A, Boldt M, Hinz S (2012) Automated detection of storm damage in forest areas by analyzing TERRASAR-X data. IGARSS 2012 Proceedings: 1672-1675, Munich

Wan HL, Jiao LC (2011) Change detection in SAR images by means of grouping connected regions using clone selection algorithm. Electronics Letters 47

Wan HL, Jung C, Hou B, Wang GT, Tang QX (2013) Novel change detection in SAR imagery using local connectivity. IEEE Geoscience and Remote Sensing Letters 10: 174-178

Wang F, Wu Y, Zhang Q, Zhang P, Li M, Lu Y (2013) Unsupervised change detection on SAR images using triplet markov field model. IEEE Geoscience and Remote Sensing Letters 10: 697-701

Zhang X, Chen J, Meng H (2013) A novel SAR image change detection based on graph-cut and generalized gaussian model. IEEE Geoscience and Remote Sensing Letters 10: 14-18

Zheng J, You H (2013) A new model-independent method for change detection in multitemporal SAR images based on radon transform and Jeffrey divergence. IEEE Geoscience and Remote Sensing Letters 10: 91-95